Comparison of Ferumoxytol based Cerebral Blood Volume Estimates using Quantitative R1 and R2* Relaxometry

Leonardo A Rivera-Rivera[1,†], **Tilman Schubert**[2,3,†], **Gesine Knobloch**[2,4], **Patrick A Turski**[1,2], **Oliver Wieben**[1,2], **Scott B. Reeder**[1,2], and **Kevin M Johnson**[1,2]

[1]Department of Medical Physics, University of Wisconsin School of Medicine and Public Health, Madison, WI, USA [2]Department of Radiology, University of Wisconsin School of Medicine and Public Health, Madison, WI, USA [3]Clinic of Radiology and Nuclear Medicine, Basel University Hospital, Basel, Switzerland [4]Department of Radiology, Charité - University Medicine, Berlin, Germany

Abstract

Purpose—Cerebral perfusion is commonly assessed clinically with dynamic susceptibility contrast magnetic resonance imaging utilizing a bolus injection of gadolinium based contrast agents, resulting in semi quantitative values of cerebral blood volume (CBV). Steady state imaging with ferumoxytol allows estimation of CBV with the potential for higher precision and accuracy. Prior CBV studies have focused on the signal disrupting T2* effects, but ferumoxytol also has high signal enhancing T1 relaxivity. The purpose of this study was to investigate and compare CBV estimation using T1 and T2*, with the goal of understanding the contrast mechanisms and quantitative differences.

Methods—Changes in R1 (1/T1) and R2* (1/T2*) were measured after the administration of ferumoxytol utilizing high-resolution quantitative approaches. Images were acquired at 3.0T and R1 was estimated from an ultrashort echo time variable flip angle approach, while R2* was estimated from a multiple gradient echo sequence. 20 healthy volunteers were imaged at two doses. CBV was derived and compared from relaxometry in gray and white matter using different approaches.

Results—R1 measurements showed a linear dependence of blood R1 with respect to dose in large vessels, in contrast to the nonlinear dose dependence of blood R2* estimates. In the brain parenchyma, R2* showed linear dose dependency whereas R1 showed nonlinearity. CBV calculations based on R2* changes in tissue and ferumoxytol blood concentration estimates based on R1 relaxivity showed the lowest variability in our cohort.

Conclusions—CBV measurements were successfully derived utilizing a combined approach of R1 and R2* relaxometry.

Keywords

Ferumoxytol; cerebral blood volume; R1; R2*; gray & white matter

INTRODUCTION

Intracranial vascular hemodynamics and vascular architecture are modified in a wide array of diseases, including tumors, stroke and varying forms of dementia (1,2). Increasing evidence exists indicating pathologic alterations of the cerebral vasculature in Alzheimer's disease (AD) and dementia with Lewy bodies patients (3–6). In light of the mounting evidence, there is a necessity to assess the cerebrovascular network. In particular, non-invasive methods capable of quantitatively assessing diffuse cerebral disease are highly desirable.

MRI enables non-invasive measurements of hemodynamics and structure in the cerebrovascular network. Blood flow is routinely assessed with phase contrast (PC) MRI (7), and contrast and non-contrast angiographic MR techniques are widely available for the evaluation of vessel structure. Cerebral perfusion can be assessed using non-contrast arterial spin labeling (ASL) or dynamic imaging during administration of an exogenous contrast agent. Clinically, cerebral perfusion is commonly assessed using gadolinium based contrast agents (GBCA) and dynamic susceptibility contrast (DSC)-MRI which exploits the T2/T2* shortening effect of the GBCA. DSC-MRI can provide estimates of cerebral blood volume (CBV) and flow (CBF) (8). DSC-MRI is also capable of detecting changes in blood vessel density and vessel size (9,10,11) and holds potential to identify tumor angiogenesis using T2-weighted 2D and 3D acquisitions (12).

Currently available GBCAs have short plasma half-lives. Thus, the current clinical standard method to assess CBV is based on T2* weighted imaging during bolus injection of GBCA. This approach requires high temporal resolution to capture the rapid arterial transit, which limits the achievable spatial resolution. Measures of CBV are derived from a joint analysis of dynamic signal from an arterial input (e.g. AIF) and the tissue of interest, and requires a conversion from signal to concentration. Such CBV measures are sensitive to the quality of arterial input measures and sensitive to errors in the concentration estimate, which arise from the diffusion of water between compartments (13,14), partial volume effects, and non-linear signal relationships. Moreover, if the blood–brain barrier is compromised, contrast can leak into the interstitium, confounding quantitative estimates of CBV. Due to these challenges, most current applications of DSC-MRI do not attempt to quantify CBV using an AIF but instead assess relative differences in CBV between different brain regions. Relative CBV measurements are subject to variations due to differing injection protocols. Using a reference region to normalize the DSC signal may improve inter-scan reproducibility; however, this assumes that regions of pathology can be readily distinguished. In chronic neurodegenerative diseases such AD, characterized by the loss of neurons in the cerebral cortex, disease may be diffuse such that drawing reference regions of interest is not practical. Absolute CBV quantification may enable the identification of global and regional pathologic CBV with higher reproducibility. Also, concerns regarding the safety of GBCAs in patients

with renal failure due to the possibility of nephrogenic systemic fibrosis (NSF), and more recently gadolinium deposition in deep brain nuclei are important considerations (15–19).

An attractive alternative for CBV assessment with MRI is the use of ferumoxytol, a dextran-coated ultra-small superparamagnetic iron oxide (USPIO) particle approved for the treatment of anemia in patients with chronic kidney disease (20). Ferumoxytol exhibits strong T1 and T2* shortening effects, has a long intravascular half-life (12–14h), and is showing promise for off-label use as an MRI contrast agent (21,22). Compared to previously proposed intravascular GBCA (23,24), ferumoxytol has much stronger T2* shortening effects. While the bolus injection of ferumoxytol is not currently recommended, steady state imaging of ferumoxytol may be used to estimate cerebrovascular parameters, such as CBV (25–27). Similar USPIOs have been successfully used in vessel size imaging studies which combine T2 and T2* weighted acquisitions, and in a DSC-MRI study for diagnosis of primary central nervous system inflammatory diseases (10,28). In 2015 the U.S. Food and Drug Administration (FDA) released a Safety Communication announcement strengthening warnings regarding the use and prescription of ferumoxytol (Feraheme) over concerns of potentially fatal allergic reactions. However, more recent studies have shown that serious adverse events are rare, and with proper precautions, ferumoxytol may be a valuable contrast agent (29–33).

A potential approach for steady-state CBV estimation with ferumoxytol is to measure changes in the effective transverse relaxation rate (R2*) pre- and post-contrast administration. This is done by assuming a linear relationship between tissue concentration of the contrast agent (CA) and R2* changes. However, CBV estimates from measurements of changes in R2* (R2*) are biased in tissues neighboring large vessels, bone or air-tissue boundaries (34). This complicates R2* based CBV estimates in the brain parenchyma, particularly in the gray matter where there is higher vessel density, and regions such as the cerebellum, which is adjacent to the bony skull base and air-tissue interfaces of the mastoid cells. While ferumoxytol studies of CBV to date have focused on the T2* effects, ferumoxytol also has high T1 relaxivity. T2* and T1 shortening effects (e.g. dynamic contrast enhanced (DCE) MRI) have substantially different mechanism to affect the extravascular signal. This presents an opportunity to probe different aspects of vascular remodeling, if accurate and co-registered T1 and T2* mapping can be achieved. For example, T1 based techniques are sensitive to water exchange with the tissue while susceptibility based techniques are not (35).

The purpose of this study was to investigate the correlation between T1 and T2* changes in brain tissue and blood, measured before and after the administration of ferumoxytol utilizing quantitative R1 and R2* relaxometry. R1 was estimated from an ultrashort echo time variable flip angle approach (UTE-VFA), simultaneously mitigating bias from flow, and T2*-decay effects; while, R2* was estimated from a multiple gradient echo sequence. In a cohort of healthy human subjects, CBV was derived and compared from relaxometry in gray and white matter using three different steady state approaches: 1) using a derived linear relationship using only R2* in tissue, 2) a combinative approach using measurements of R2* in tissue and R1 in blood and finally 3) by fitting a two-compartment water exchange limited relaxation model using R1 in tissue and blood.

METHODS

Subjects

22 healthy subjects (age range 20–61y, mean=32y, 12F) were prospectively recruited from an Institutional Review Board (IRB) approved database. This study was Health Insurance Portability and Accountability Act (HIPAA) compliant and the local Institutional Review Board (IRB) approved all study procedures and protocols following the policies and guidance established by the campus Human Research Protection Program (HRPP). Each participant provided signed informed consent before participation. The administration of ferumoxytol followed recently published guidelines on the safe use of ferumoxytol for research (22).

MR Imaging Protocol

3D volumetric MRI images were acquired using UTE-VFA T1 and multi echo T2* mapping sequences on a 3.0T scanner (MR750, GE Healthcare Waukesha, WI, USA) with a 32ch head coil (Nova Medical, Wilmington, MA, USA). For all subjects, scanning was performed before and after the administration of two doses of ferumoxytol. Ferumoxytol was diluted at least 5-fold up to 60 mL in normal saline, and injected as a slow infusion. Images were acquired at 3 time points: 1) pre-contrast, 2) after a first injection (1mgFE/kg) and 3) after a second injection (4mgFE/kg), for a total ferumoxytol dose of 5mgFE/kg. The timing between the two ferumoxytol injections ranged from 15 to 20 minutes for all subjects. UTE-VFA images were acquired using a 3D radial sampling trajectory with the following imaging parameters: TE/TR = 0.2/3.6ms, flip angles = 2°,8°,14°,20°, imaging volume=240×240×240mm^3, projection number = 22 932, 0.94mm isotropic resolution and scan time = 5:11min (36,37). Actual flip angle (AFI) images were also acquired from which B1 maps were generated (38). 3D multi-echo gradient echo images using a Cartesian sampling trajectory were acquired with: TR= 32.5ms, 8 equally spaced echo times acquired in a single TR, ranging from 2.2ms to 29.8ms, flip angle = 15°, 1mm isotropic resolution, FOV=256×180×240mm^3 and scan time = 5:00min.

Post processing

B1 maps generated from AFI images were combined with the fitting of the UTE-VFA images to obtain R1 (1/T1) images. R2* (1/T2*) images were generated from complex fitting of the multi-echo images, fitting for the off-resonance, R2*, and signal density. Both R2* and R1 fitting was performed with a multi-resolution search of complex images coil-combined with the method proposed by Walsh et al (39). A total of 6 sets of images were generated per subject, R1 and R2* maps for each of the 3 ferumoxytol concentrations (pre-contrast, 1 mg FE/kg, 5 mg FE/kg). Images were co-registered in MATLAB (The Mathworks, Natick, MA) using a rigid body registration utilizing the source images. Subjective reader assessment for image quality was performed by two radiologists (1 senior neuro-radiologist (>30 years of experience) and 1 radiologist (>10 years of experience)). For each subject, partial volume masks (PVMs) of gray matter (GM) and white matter (WM) were generated in FMRIB's Automated Segmentation Tool in the FSL software library package from the registered pre-contrast R1 and R2* images (40). A combined R1 and R2* segmentation approach was used to avoid possible confounding errors in R1 and R2*

measurements in tissues due to presence of nearby vessels. Additionally, to improve tissue segmentation, non-brain tissue was removed from the R1 and R2* images before generating the PVMs using the Brain Extraction Tool in FSL (41). PVMs were converted to binary masks in MATLAB by assigning a value of 1 to voxels with at least 95% GM or WM, and 0 to the remaining voxels. The GM and WM masks were further eroded by a single voxel using ImageJ (National Institute of Health, Bethesda, MD). Finally, to measure local R1 and R2* values, the GM and WM masks were combined with the R1 and R2* images. In order to estimate the R1 and R2* values of blood, a region of interest was manually drawn in the superior sagittal sinus (42). Measurements in the sinus were averaged over 5 slices. Pixel wise changes were analyzed in the registered images and cumulated into 2D histograms. These data were projected along the R1 and R2* values at two different doses concentration 1mgFE/kg and 5mgFE/kg.

CBV estimation

CBV in tissue was estimated using steady-state approaches using R2* data alone, R2* data with blood concentration from R1 data, and from R1 data alone. From R2* data, CBV was estimated using the assumption of static dephasing using a model of randomly oriented cylinders previously described analytically and verified in Monte Carlo simulations (10,43,44). In this approach CBV is given by:

$$CBV_{SS} = \frac{3\Delta R_2^*}{4\pi\gamma\Delta\chi_{USPIO}B_0} \quad (1)$$

Where CBV has units of fraction of blood in tissue, ΔR_2^* is the measured change in tissue relaxation rate, γ is the proton gyromagnetic ratio equal to 2.675×10^8 rad/s/T, B_0 is the main magnetic field and $\Delta\chi_{USPIO}$ is the change of magnetic susceptibility of blood after injection of ferumoxytol, and is given by:

$$\Delta\chi_{USPIO} = C_b\frac{M_{sat}}{B_0} \quad (2)$$

Where M_{sat} is the saturation magnetization of ferumoxytol, and is equal to 0.396 μT/mM of iron and C_b is the concentration of ferumoxytol in blood (mM = mmol/L) (45–47). Two approaches were used to estimate C_b. The first approach uses the formula:

$$C_b = \frac{m_{FE}}{M_{Fe}\,TBV} \quad (3)$$

M_{Fe} is the standard atomic weight of iron, m_{FE} the injected mass of ferumoxtyol and TBV is the total blood volume computed using Nadler's formula (48). The second approach used to estimate C_b is given by:

$$C_b = \frac{\Delta R_{1blood}}{r_1} \quad (4)$$

Where $\Delta R_{1\ blood}$, the measured change in blood relaxation rate, was used to estimate the concentration of ferumoxytol in blood by exploiting the linear relationship of R1 in blood and ferumoxytol concentration. The R1 relaxivity of ferumoxytol in blood, i.e. r_1, at 3.0T was determined in ex vivo experiments and was equal to 8.6725 $s^{-1}mM^{-1}$. The linear correlation between R_{1blood} and concentration of contrast agent in blood C_b, was investigated in ex vivo experiments at 3.0T using ferumoxytol in whole human blood with hematocrit = 42%. The manuscript on the report of that study is in preparation for publication elsewhere.

CBV was also estimated using R1 in blood and tissue by fitting a two-compartment water exchange limited relaxation model (49). This model gives a quantitative description of the effect of relative CBV and intra-/extravascular water exchange rates on the effective tissue longitudinal tissue relaxation rates. Using this model, it can be shown that the Bloch equation, including terms for the two-compartment water exchange, has the following solution for R1 (49):

$$R_1 = 0.5 \left(R_{1b} + \frac{PS}{CBV} + R_{1e} + \frac{PS}{\lambda - CBV} \right) - 0.5 \sqrt{ \left(R_{1b} + \frac{PS}{CBV} - R_{1e} - \frac{PS}{\lambda - CBV} \right)^2 + \frac{4PS^2}{CBV(\lambda - CBV)} }$$

$$(5)$$

where R1 is the measured tissue relaxation rate; R1b and R1e are the relaxation rates in blood and the extravascular space, respectively; PS is the water permeability surface area product between the intra-/extravascular space; CBV is the cerebral blood volume; and λ, which is the ratio of the proton spin densities of tissue and blood, is assumed to be 0.9, similar to the previously reported value (49). The PS product was derived with units of mL/sec/g tissue, and CBV with units of fraction of blood in tissue (represented as mL/100 g tissue), to follow the literature convention (49), by assuming a tissue density of 1 g/mL. The CBV units for both R2* and R1 based analysis are equivalent.

To determine the PS product, R1e and CBV values, a three-parameter, nonlinear least squares fit was applied to equation (5), using 3 data points (0, 1mg FE/kg, and 5mg FE/kg doses). A limitation of fitting R1 to a two-compartment water exchange model is the uncertainty in the measured PS product. This tissue-dependent value will vary with individual subjects and is not easily measurable in a clinical setting (13,14). To investigate the uncertainty in the measured PS product, the parameter τ_b can be defined as the ratio of CBV and PS product. τ_b is the capillary water molecule lifetime and is given by:

$$\tau_b = \frac{CBV}{PS} \quad (6)$$

Assuming a fixed value for τ_b, a two-parameter fit can be performed to estimate CBV and R1e using equation (5) and the R_1 measurements at two different ferumoxytol concentrations (0 and 5mg FE/kg).

Statistical Analysis

Values of CBV estimates were compared between gray and white matter for all subjects. The differences between gray and white matter CBV estimates was assessed using ANOVA followed by Tukey-Kramer method for pairwise comparison for adjusted means. The R1 and R2* measurements used to estimate CBV are represented by the median value from histograms containing signal values from voxels from tissue after segmentation of WM and GM. Statistical analysis was performed in MATLAB. $P < 0.05$ was set as the threshold for statistical significance.

RESULTS

From 22 enrolled volunteers, 20 subjects completed the study protocol (age range 20–61y, mean=32y, 11F). One subject's scan session was incomplete due to hard drive storage failure in the MRI system console. Data from another subject were not included due to incomplete acquisition of the data, resulting from the subject not responding to instructions from the technician and the scan stopped to assess the subject's condition. The subject's vital signs were immediately checked and were normal. The subject was oriented and appeared to be in no distress but the scan was not completed to allow for continued observation. The subject was released after one hour and was symptom free.

Representative R2*, R1, R2*, and R1 images from a single slice of the volume from one subject are shown in Figure 1. R1 and R2* images were acquired at a similar spatial resolution; however, R2* estimates are susceptible to signal loss from static gradients from large vessels, which is visually apparent. R1 estimates are unaffected by this artifact. R2* based imaging provides more sensitivity; however, vessels are depicted better in R1 albeit a lower SNR (9,50,51). The R1 images provide better contrast between GM, WM and cerebral spinal fluid (CSF) than R2* images, although R2* images were more sensitive to show voxels containing vessels, as observed in the images histogram. Overall, however, there is good subjective agreement between the 3D UTE-VFA T1 and 3D R2* mapping techniques, especially at the higher doses.

R1 and R2* estimates in WM and GM are summarized in Figure 2. The R1 estimates (a) show a weaker correlation with dose-response at high concentrations of ferumoxytol, with a coefficient of determination $R^2 = 0.27$ in WM and 0.71 in GM. R2* (b) exhibits a stronger dose response in tissue having a coefficient of determination $R^2 = 0.91$ for both GM and WM. Figure 3 shows the R1 (a) and R2* (b) measurements observed in a blood vessel (superior sagittal sinus) across all subjects. In large vessels R2* exhibits a non-linear

response to dose, in contrast with a linear relationship between dose and R2* found in tissue. A quadratic model fit the data best with an adjusted coefficient of determination $R^2_{adj} = 0.86$, while R1 in blood exhibits a linear response to dose of ferumoxytol with $R^2 = 0.96$ for the linear fit.

Voxel wise relationship between ΔR2* and ΔR1 estimates for 1mg FE/kg and 5 mg FE/kg dose of ferumoxytol are shown in figure 4 for all subjects. When plotting ΔR1 vs ΔR2*, the ΔR1 (a, b) shows a wide range of variation where ΔR2* does not change. It should be noted that there are fewer voxels with these values, as partially indicated by the wider quartile range. When plotting ΔR2* vs ΔR1, ΔR2* (c, d) tends to exhibit changes where the ΔR1 does not change, suggesting the susceptibility effect of blood is non-local (e.g. dipole kernel convolution), and thus affects low CBV tissues and the vessel size is overestimated in R2* images. 2D histograms for specific tissue type (GM and WM) were also investigated (Supporting Fig. S1). For WM tissue the 2D histogram shows initially a faster increase in ΔR2* than ΔR1. The dependence of R1 estimates in blood with body mass index (BMI) at 3 different concentrations of ferumoxytol was investigated. Although there were variations in R1 of the blood among subjects, no correlations in R1 blood vs BMI were found, suggesting variation in R1 beyond those due to BMI (Supporting Fig. S2).

Results of the CBV estimates are summarized in figure 5. When using ΔR2* from tissue to estimate CBV and the TBV calculation to estimate concentration of CA in blood, the mean values of CBV were 3.1 ± 0.5 % in GM and 1.6 ± 0.2 % in WM. Instead, if C_b is estimate from the R1 in blood, the mean values of CBV are 3.7 ± 0.5 % in GM and 1.8 ± 0.2 % in WM. Finally, the CBV estimates from using R1 in blood and tissue to fit the two-compartment water exchange limited relaxation model were the lowest with averages of 2.0 ± 0.9 mL/100 g GM and 1.2 ± 0.9 mL/100 g WM tissue. CBV estimates in GM were significantly larger than CBV estimates in WM for the three approaches. The relaxation rate in the extravascular space (R1e) was 0.53 ± 0.03 s^{-1} in GM and 0.83 ± 0.04 s^{-1} in WM. The median value of the water permeability surface area product between the intra-/extravascular space PS was 0.259 ± 0.079 mL/s/g GM and 0.194 ± 0.118 mL/s/g WM tissue. Least squares curve fit to the water exchange limited relaxation model in GM and WM for all subjects (n=20) are shown in supporting figures S3 and S4. To investigate the uncertainty in the PS product, the parameter τ_b was fixed while fitting the two-compartment water exchange model. Using CBV estimated from the ΔR2* approaches, τ_b was measured to be 0.233 ± 0.012 s. R1 based CBV measures were then estimated using a fixed τ_b (0.233 s) and a two parameter fit of the two-compartment water exchange limited relaxation model resulting in CBV values of 3.7 ± 0.7 mL/100 g GM and 1.9 ± 0.8 mL/100 g WM tissue.

DISCUSSION AND CONCLUSIONS

In this study, we investigated changes in cerebral R1 and R2* relaxometry before and after the administration of two escalating doses of ferumoxytol in a cohort of 20 healthy volunteers. The main findings of this study are a linear dependence of blood R1 with respect to dose in large vessels, in contrast to the nonlinear dose dependence of blood R2* estimates. In the brain parenchyma, however, R2* showed linear dose dependency whereas R1 showed nonlinearity and signal saturation at higher doses. Finally, CBV estimates using

different approaches to calculate ferumoxytol concentration in blood showed consistent values with statistically significant higher CBV estimates in GM when compared to CBV estimates in WM, similar to values reported in other studies (45). CBV calculations based on R2* changes in tissue and ferumoxytol blood concentration estimates based on R1 relaxivity showed the lowest variability in our cohort.

The non-linear response to concentration in tissue remains a challenge in measuring CBV from R1 relaxometry alone. This does not arise from a limited dynamic range of the R1 sequence, given the wide range of flip angles used and the application of an ultrashort echo time readout, but rather the intrinsic complexity and nonlinearity of the relationship between the apparent R1 in tissue and ferumoxytol concentration. Since the relaxation effect of the agent only affects protons within a very close proximity of the USPIO, rapid water exchange is required to carry the relaxation effects of the contrast agent beyond the plasma compartment (52,53). The linear behavior of R1 in blood as a function of dose implies that the intra-/extracellular water exchange rate with red blood cells is much faster than the intra-/extravascular exchange rate (14). Similar R1 behavior in tissue and blood using a different USPIO has been observed in pig experiments (54). While the two compartment fit is expected to correct for these factors, the fitting is challenging due to the sensitivity to the water permeability surface area product between the intra-/extravascular space.

The non-linear dose dependence of R2* in blood is a major challenge when estimating CBV from R2* relaxometry alone. For example, different R2* relaxation responses to USPIO were found in tissue and blood. In blood, R2* has a nonlinear dependence on dose (R^2_{adj}=0.86 for quadratic fit), but in tissue it scales linearly ($R^2 = 0.91$) with ferumoxytol concentration in both GM and WM. Similar findings have been reported in previous studies investigating R2* relaxation using ferumoxytol with multi-echo R2* mapping approaches (25). The non-linear behavior of R2* in blood can make estimation of contrast agent concentration in blood challenging, whereas the linear behavior in tissue makes R2* a better estimate of blood volume in tissue and was used in the steady state approach CBV estimations.

The pixel correlation plots in figure 4 show that further complexities exist in the comparison of R2* and R1 signal changes. When plotting ΔR2* vs ΔR1, ΔR2* increases in areas where ΔR1 does not exhibit changes (i.e. ΔR1=0). This is observed in tissues such as CSF and around vessels, suggesting that the non-local effects of susceptibility changes (e.g. vessel blooming) may contribute to the ΔR2* increase in those voxels. As there are few pixels in which R2* does not change following injection, the pixel wise correlations of ΔR1 with ΔR2* (figure 4. a, b) initially show a large amount of variability. After this region, ΔR1 increases monotonically with ΔR2*. However, the ΔR1 behavior is not linear with smaller relative changes in ΔR1 at higher values of ΔR2*. A similar behavior can be observed at high ΔR1, where the rate ΔR2* increase diminishes. Many of these voxels are those containing small and medium sized vessels, where the dose response is non-linear and less sensitive to those in the capillary bed. These effects obfuscate the correlation of ΔR2* and ΔR1 outside of homogenous tissues such as gray matter and white matter.

CBV estimates in gray and white matter (figure 5) agree well with previous studies that also estimated CBV by exploiting R2* linearity of ferumoxtyol in tissue using a steady state approach (45). The CBV values were higher in both GM and WM when blood R1 were used to estimate ferumoxytol concentration in blood. The resulting CBV estimates using this method are closer to CBV estimates derived from PET (55). If exclusively R1 from blood and tissue are used to estimate CBV, then a two-compartment water exchange limited relaxation model can be fit. The CBV estimation from fitting a two-compartment water exchange limited relaxation model were similar in WM but lower in GM when compared to another study that used the same model but a multi echo imaging technique at 7 T and GBCA (56). A possible reason for these differences might be due to the fact that the mentioned study used multiple data points per subject to perform the 3 parameter fitting whereas in this study only 3 points were available per subject. Furthermore, the referenced study used DCE-MRI with a GBCA. A limitation of fitting R1 measurements to a two-compartment water exchange model, is the uncertainty in the measured *PS* product or water permeability surface area product between the intra-/extravascular space. As mention before, this value will depend on tissue and is not easily measured due to a high level of sensitivity to noise. This occurs since at low concentrations, the observed change in R1 is relatively similar for an increase in CBV or an increase in PS. To investigate how the uncertainty in the PS product affects the variance in the blood volume results, the parameter τ_b was estimated. The resulting CBV estimates showed a significant decrease in the spread of the data for both GM and WM. This illustrates the large PS product uncertainty affects the spread in the CBV estimates from fitting a two-compartment water exchange limited relaxation model. This limitation makes the combination of R2* linearity in tissue to estimate CBV and the linearity of R1 in blood to estimate CA concentration more reproducible in a clinical setting. However, even with the limited number of data points to fit the two-compartment water exchange relaxation model the derived values of water PS product and CBV were reproducible and describe the measured tissue R1. Additionally, the two compartment water exchange model implicitly assumes that the tissue vascular fraction is small such that the tissue R1 recovery curve is approximately monoexponential at all values of R1b.

The R1 values measured using the UTE-VFA technique demonstrated a high degree of correlation with R2* estimates and was highly effective in large vessels. The ability to depict large vessel changes and the potential to probe permeability changes suggest that this technique may be of value when combined with susceptibility based measures. UTE-VFA is well suited to capture the linear dose dependence of R1 after ferumoxtyol administration in blood due to short echo times. Furthermore, UTE –based T1 approaches using USPIO to generate CBV estimates have been successfully implemented in rat models recently (57).

The proposed work showed several possible techniques to quantify CBV from ferumoxytol with increasing complexity. As a straightforward approach, R2* can be measured in tissue and the concentration of blood can be estimated from population averages (e.g. Nadler's equation). R2* mapping is readily available on all vendor scanners and has been widely used in other organs. R2* has the advantage of being approximately linear in tissue but the disadvantage of being unable to probe water exchange and sensitivity to variation in total blood volume. The use of R1 is attractive due to the potential to accurately quantify the concentration of blood and investigate water exchange. However, R1 mapping is

significantly more complex than R2* mapping, most notably it is sensitive to B1 variations. Recent progress in this area have suggest a vast array of techniques to correct and compensate for B1 ranging from separate scan calibration techniques (58), as used here, to MR fingerprinting approaches with B1 incorporation (59). Our results suggest the most accurate quantification requires both techniques. This adds additional scan time to the imaging protocol and more work is required to reduce these imaging times to those that are more clinically manageable. As ferumoxytol currently requires a slowly infused bolus, protocols should be designed which allow imaging during this infusion.

There are a number of limitations in this study. First, the hematocrit levels of brain tissue were not incorporated in the CBV estimates calculations. We assume R1 in blood and plasma are similar. Recently, new methods have been proposed to estimate hematocrit analytically (60). Ideally, more data points should be used to fit the R1 in a blood and tissue two-compartment water exchange limited relaxation model. This study was limited to 3 points per subject, which might explain the lower CBV estimates when compared to the steady state R2* models. One potential limitation of R2/R2* based techniques is that they have reduced sensitivity as the vessel size is reduced below 10 μm. This arises from a transition to the diffusional narrowing regime from our assumed static dephasing regime. R2* gradient echo (GRE) based techniques have a sensitivity plateau at vessel diameters of 10μm and larger. Thus in this study, the blood volume fraction measured in the brain parenchyma using the R2*-based method does not include all the contribution from the capillary vessel network (3–5 microns). The major contribution measured were from small-to-large vessels and some capillaries. The actual impact of vessel size is difficult to gauge as the effect is small compared to the variability in reference standard measurements, such as those derived from PET. The use of spin-echo based (T2) imaging would provide an opportunity to reduced sensitivity to larger vessel diameters (9,50,51) but exhibits a similar loss in sensitivity as the vessel diameter is reduced.

In summary, in this work we investigated the correlation between relaxometry changes in R1 and R2* measured after the administration of ferumoxytol utilizing quantitative T1 and T2* imaging approaches in healthy volunteers. R1 was estimated from an ultrashort echo time variable flip angle approach (UTE-VFA), whereas R2* was estimated using a multi-echo approach. Finally, CBV measurements were successfully derived for GM and WM utilizing a combined approach of R1 and R2* relaxometry, exploiting the linearity and accuracy of dose dependent R1 values in blood vessels and the higher signal sensitivity of R2* values in tissue.

Supplementary Material

Refer to Web version on PubMed Central for supplementary material.

Acknowledgments

References

1. Law M, Yang S, Babb JS, Knopp EA, Golfinos JG, Zagzag D, Johnson G. Comparison of cerebral blood volume and vascular permeability from dynamic susceptibility contrast-enhanced perfusion MR imaging with glioma grade. AJNR Am J Neuroradiol. 2004; 25:746–755. [PubMed: 15140713]

2. Hachinski V, Iadecola C, Petersen RC, et al. National Institute of Neurological Disorders and Stroke-Canadian Stroke Network vascular cognitive impairment harmonization standards. Stroke. 2006; 37:2220–2241. [PubMed: 16917086]

3. Roher AE. Cardiovascular system participation in Alzheimer's disease pathogenesis. J Intern Med. 2015; 277:426–428. [PubMed: 25251680]

4. Rivera-Rivera LA, Turski P, Johnson KM, Hoffman C, Berman SE, Kilgas P, Rowley HA, Carlsson CM, Johnson SC, Wieben O. 4D flow MRI for intracranial hemodynamics assessment in Alzheimer's disease. J Cerebr Blood Flow Metab. 2016 Oct; 36(10):1718–1730.

5. Rivera-Rivera LA, Schubert T, Turski P, Johnson KM, Berman SE, Rowley HA, Carlsson CM, Johnson SC, Wieben O. Changes in intracranial venous blood flow and pulsatility in Alzheimer's disease: A 4D flow MRI study. J Cereb Blood Flow Metab. 2017 Jun; 37(6):2149–2158. [PubMed: 27492950]

6. Deramecourt V, Slade JY, Oakley AE, Perry RH, Ince PG, Maurage CA, Kalaria RN. Staging and natural history of cerebrovascular pathology in dementia. Neurology. 2012 Apr 3; 78(14):1043–1050. [PubMed: 22377814]

7. Lee VS, Spritzer CE, Carrol BA, Pool LG, Bernstein MA, Heinle SK, MacFall JR. Flow quantification using fast cine phase-contrast MR imaging, conventional cine phase-contrast MR imaging, and Doppler sonography: in vitro and in vivo validation. AJR Am J Roentgenol. 1997 Oct; 169(4):1125–31. [PubMed: 9308476]

8. Østergaard L. Principles of cerebral perfusion imaging by bolus tracking. J Magn Reson Imaging. 2005; 22:710–717. [PubMed: 16261573]

9. Kiselev VG, Strecker R, Ziyeh S, Speck O, Hennig J. Vessel size imaging in humans. Magn Reson Med. 2005; 53:553–63. [PubMed: 15723391]

10. Troprès I, Grimault S, Vaeth A, Grillon E, Julien C, Payen JF, Lamalle L, Décorps M. Vessel size imaging. Magn Reson Med. 2001; 45:397–408. [PubMed: 11241696]

11. Emblem KE, Mouridsen K, Bjornerud A, et al. Vessel architectural imaging identifies cancer patient responders to anti-angiogenic therapy. Nat Med. 2013 Sep; 19(9):1178–1183. [PubMed: 23955713]

12. Maia AC Jr, Malheiros SM, da Rocha AJ, da Silva CJ, Gabbai AA, Ferraz FA, Stávale JN. MR cerebral blood volume maps correlated with vascular endothelial growth factor expression and tumor grade in nonenhancing gliomas. AJNR Am J Neuroradiol. 2005 Apr; 26(4):777–83. [PubMed: 15814920]

13. Donahue KM, Weisskoff RM, Chesler DA, Kwong KK, Bogdanov AA Jr, Mandeville JB, Rosen BR. Improving MR quantification of regional blood volume with intravascular T1 contrast agents: accuracy, precision, and water exchange. Magn Reson Med. 1996; 36:858–867. [PubMed: 8946351]

14. Donahue KM, Weisskoff RM, Burstein D. Water diffusion and exchange as they influence contrast enhancement. J Magn Reson Imaging. 1997 Jan-Feb;7(1):102–10. [PubMed: 9039599]

15. Agarwal R, Brunelli SM, Williams K, Mitchell MD, Feldman HI, Umscheid CA. Gadolinium-based contrast agents and nephrogenic systemic fibrosis: a systematic review and meta-analysis. Nephrol Dial Transplant. 2009 Mar; 24(3):856–63. [PubMed: 18952698]

16. Weinreb JC, Abu-Alfa AK. Gadolinium-based contrast agents and nephrogenic systemic fibrosis: why did it happen and what have we learned? J Magn Reson Imaging. 2009 Dec; 30(6):1236–9. [PubMed: 19938035]

17. Kanal E, Tweedle MF. Residual or retained gadolinium: practical implications for radiologists and our patients. Radiology. 2015; 275(3):630–634. [PubMed: 25942418]

18. Radbruch A, Weberling LD, Kieslich PJ, Eidel O, Burth S, Kickingereder P, Heiland S, Wick W, Schlemmer HP, Bendszus M. Gadolinium retention in the dentate nucleus and globus pallidus is dependent on the class of contrast agent. Radiology. 2015; 275(3):783–791. [PubMed: 25848905]

19. Gulani V, Calamante F, Shellock FG, Kanal E, Reeder SB. Gadolinium deposition in the brain: summary of evidence and recommendations. Lancet Neurol. 2017 Jul; 16(7):564–570. [PubMed: 28653648]

20. Li W, Tutton S, Vu AT, Pierchala L, Li BS, Lewis JM, Prasad PV, Edelman RR. First-pass contrast-enhanced magnetic resonance angiography in humans using ferumoxytol, a novel ultrasmall superparamagnetic iron oxide (USPIO)-based blood pool agent. J Magn Reson Imaging. 2005 Jan; 21(1):46–52. [PubMed: 15611942]

21. Bashir MR, Bhatti L, Marin D, Nelson RC. Emerging applications for ferumoxytol as a contrast agent in MRI. J Magn Reson Imaging. 2015 Apr; 41(4):884–98. [PubMed: 24974785]

22. Vasanawala SS, Nguyen KL, Hope MD, Bridges MD, Hope TA, Reeder SB, Bashir MR. Safety and technique of ferumoxytol administration for MRI. Magn Reson Med. 2016 May; 75(5):2107–11. [PubMed: 26890830]

23. Rohrer M, Bauer H, Mintorovitch J, Requardt M, Weinmann HJ. Comparison of magnetic properties of MRI contrast media solutions at different magnetic field strengths. Invest Radiol. 2005 Nov; 40(11):715–24. [PubMed: 16230904]

24. Richardson OC, Scott MLJ, Tanner SF, Waterton JC, Buckley DL. Overcoming the Low Relaxivity of Gadofosveset at High Field with Spin Locking. Magnetic Resonance in Medicine. 2012 Oct. 68:1234–1238. (2012). [PubMed: 22161901]

25. Christen T, Ni W, Qiu D, Schmiedeskamp H, Bammer R, Moseley M, Zaharchuk G. High-resolution cerebral blood volume imaging in humans using the blood pool contrast agent ferumoxytol. Magn Reson Med. 2013 Sep; 70(3):705–10. [PubMed: 23001902]

26. Pohlmann A, Karczewski P, Ku MC. Cerebral blood volume estimation by ferumoxytol-enhanced steady-state MRI at 9.4 T reveals microvascular impact of α1 - adrenergic receptor antibodies. NMR Biomed. 2014 Sep; 27(9):1085–93. [PubMed: 25060359]

27. Varallyay CG, Nesbit E, Fu R, Gahramanov S, Moloney B, Earl E, Muldoon LL, Li X, Rooney WD, Neuwelt EA. High-resolution steady-state cerebral blood volume maps in patients with central nervous system neoplasms using ferumoxytol, a superparamagnetic iron oxide nanoparticle. J Cereb Blood Flow Metab. 2013 May; 33(5):780–6. [PubMed: 23486297]

28. Farrell BT, Hamilton BE, Dósa E, et al. Using iron oxide nanoparticles to diagnose CNS inflammatory diseases and PCNSL. Neurology. 2013 Jul 16; 81(3):256–263. [PubMed: 23771486]

29. FDA Drug Safety Communication: FDA strengthens warnings and changes prescribing instructions to decrease the risk of serious allergic reactions with anemia drug Feraheme (ferumoxytol). Food and Drug Administration (FDA); website. https://www.fda.gov/Drugs/DrugSafety/ucm440138.htm. Published March 30, 2015. Accessed July 24, 2017

30. Varallyay CG, Toth GB, Fu R, et al. What Does the Boxed Warning Tell Us? Safe Practice of Using Ferumoxytol as an MRI Contrast Agent. AJNR Am J Neuroradiol. 2017 Jul; 38(7):1297–1302. [PubMed: 28495944]

31. Muehe AM, Feng D, von Eyben R, et al. Safety Report of Ferumoxytol for Magnetic Resonance Imaging in Children and Young Adults. Invest Radiol. 2016 Apr; 51(4):221–7. [PubMed: 26656202]

32. Nguyen KL, Yoshida T, Han F, et al. MRI with ferumoxytol: a single center experience of safety across the age spectrum. J Magn Res Imaging. 2017; 45:804–12.

33. Finn JP, Nguyen KL, Hu P. Ferumoxytol vs. Gadolinium agents for contrast-enhanced MRI: Thoughts on evolving indications, risks, and benefits. J Magn Reson Imaging. 2017 Sep; 46(3): 919–923. [PubMed: 28160356]

34. Kim SG, Harel N, Jin T, Kim T, Lee P, Zhao F. Cerebral Blood Volume MRI with Intravascular Superparamagentic Iron Oxide Nanoparticles. NMR Biomed. 2013 Aug; 26(8):949–962. [PubMed: 23208650]

35. Larsson HB, Rosenbaum S, Fritz-Hansen T. Quantification of the effect of water exchange in dynamic contrast MRI perfusion measurements in the brain and heart. MagnReson Med. 2001 Aug; 46(2):272–81.

36. Tyler DJ, Robson MD, Henkelman RM, Young IR, Bydder GM. Magnetic Resonance Imaging With Ultrashort TE(UTE) PULSE Sequences: Technical Considerations. J Magn Reson Imaging. 2007 Feb; 25(2):279–89. [PubMed: 17260388]

37. Cheng HL, Wright GA. Rapid high-resolution T(1) mapping by variable flip angles: accurate and precise measurements in the presence of radiofrequency field inhomogeneity. Magn Reson Med. 2006 Mar; 55(3):566–74. [PubMed: 16450365]

38. Yarnykh VL. Actual Flip-Angle Imaging in the Pulsed Steady State: A Method for Rapid Three-Dimensional Mapping of the Transmitted Radiofrequency Field. Magnetic Resonance in Medicine. 2007; 57:192–200. [PubMed: 17191242]

39. Walsh DO, Gmitro AF, Marcellin MW. Adaptive Reconstruction of Phased Array MR Imagery. Magnetic Resonance in Medicine. 2000; 43:682–690. [PubMed: 10800033]

40. Zhang Y, Brady M, Smith S. Segmentation of brain MR images through a hidden Markov random field model and the expectation-maximization algorithm. IEEE Trans Med Imag. 2001; 20(1):45–57.

41. Smith SM. Fast robust automated brain extraction. Human Brain Mapping. Nov; 2002 17(3):143–155. [PubMed: 12391568]

42. Zhao JM, Clingman CS, Närväinen MJ, Kauppinen RA, van Zijl PC. Oxygenation and hematocrit dependence of transverse relaxation rates of blood at 3T. Magn Reson Med. 2007 Sep; 58(3):592–7. [PubMed: 17763354]

43. Yablonskiy DA, Haacke EM. Theory of NMR signal behavior in magnetically inhomogeneous tissues: the static dephasing regime. Magn Reson Med. 1994 Dec; 32(6):749–63. [PubMed: 7869897]

44. Kjølby BF, Østergaard L, Kiselev VG. Theoretical model of intravascular paramagnetic tracers effect on tissue relaxation. Magn Reson Med. 2006 Jul; 56(1):187–97. [PubMed: 16724299]

45. Christen T, Pannetier NA, Ni W, Qiu D, Moseley ME, Schuff N, Zaharchuk G. MR Vascular Fingerprinting: A New Approach to Compute Cerebral Blood Volume, Mean Vessel Radius, and Oxygenation Maps in the Human Brain. Neuroimage. 2014 Apr 1.89:262–270. [PubMed: 24321559]

46. Barick KC, Aslam M, Lin YP, Prasadd PV, Dravid VP. Novel and efficient MR active aqueous colloidal Fe3O4 nanoparticle assemblies. J Mater Chem. 2009; 19:7023–7029.

47. Tan H, Liu T, Wu Y, et al. Evaluation of iron content in human cerebral cavernous malformation using quantitative susceptibility mapping. Invest Radiol. 2014 Jul; 49(7):498–504. [PubMed: 24619210]

48. Nadler SB, Hidalgo JH, Bloch T. Prediction of blood volume in normal human adults. Surgery. 1962; 51:224–232. [PubMed: 21936146]

49. Schwarzbauer C, Morrissey SP, Deichmann R, Hillenbrand C, Syha J, Adolf H, Nöth U, Haase A. Quantitative magnetic resonance imaging of capillary water permeability and regional blood volume with an intravascular MR contrast agent. Magn Reson Med. 1997 May; 37(5):769–77. [PubMed: 9126952]

50. Schmiedeskamp H, Straka M, Newbould RD, Zaharchuk G, Andre JB, Olivot JM, et al. Combined spin- and gradient-echo perfusion-weighted imaging. Magn Reson Med. 2012; 68:30–40. [PubMed: 22114040]

51. Speck O, Chang L, DeSilva NM, Ernst T. Perfusion MRI of the human brain with dynamic susceptibility contrast: gradient-echo versus spin-echo techniques. J Magn Reson Imaging. 2000; 12:381–387. [PubMed: 10992304]

52. Koenig SH, Kellar KE. Theory of proton relaxation in solutions of magnetic nanoparticles, including the superparamagnetic size range. Acad Radiol. 1996; 3(Suppl 2):S273–S276. [PubMed: 8796579]

53. Gossuin Y, Roch A, Muller RN, Gillis P. Relaxation induced by ferritin and ferritin-like magnetic particles: the role of proton exchange. Magn Reson Med. 2000 Feb; 43(2):237–43. [PubMed: 10680687]

54. Bjørnerud A, Johansson LO, Briley-Sæbø K, Ahlström HK. Assessment of T1 and T*2 Effects In Vivo and Ex Vivo Using Iron Oxide Nanoparticles in Steady State-Dependence on Blood Volume and Water Exchange. Magn Reson Med. 2002 Mar; 47(3):461–71. [PubMed: 11870832]

55. Leenders KL, Perani D, Lammertsma A, et al. Cerebral blood flow, blood volume and oxygen utilization normal values and effect of age. Brain. 1990; 113:27–47. [PubMed: 2302536]

56. Rooney WD, Li X, Sammi MK, Bourdette DN, Neuwelt EA, Springer CS Jr. Mapping human brain capillary water lifetime: high-resolution metabolic neuroimaging. NMR Biomed. 2015 Jun; 28(6):607–23. [PubMed: 25914365]

57. Han SH, Cho JH, Jung HS, Suh JY, Kim JK, Kim YR, Cho G, Cho H. Robust MR assessment of cerebral blood volume and mean vessel size using SPION-enhanced ultrashort echo acquisition. Neuroimage. 2015 May 15.112:382–9. DOI: 10.1016/j.neuroimage.2015.03.042 [PubMed: 25818683]

58. Hurley SA, Yarnykh VL, Johnson KM, Field AS, Alexander AL, Samsonov AA. Simultaneous variable flip angle-actual flip angle imaging method for improved accuracy and precision of three-dimensional T1 and B1 measurements. Magn Reson Med. 2012 Jul; 68(1):54–64. [PubMed: 22139819]

59. Buonincontri G, Sawiak SJ. MR fingerprinting with simultaneous B1 estimation. Magn Reson Med. 2016 Oct; 76(4):1127–35. [PubMed: 26509746]

60. Portnoy S, Seed M, Sled JG, Macgowan CK. Non-invasive evaluation of blood oxygen saturation and hematocrit from T1 and T2 relaxation times: In-vitro validation in fetal blood. Magn Reson Med. 2017 Feb 12.doi: 10.1002/mrm.26599
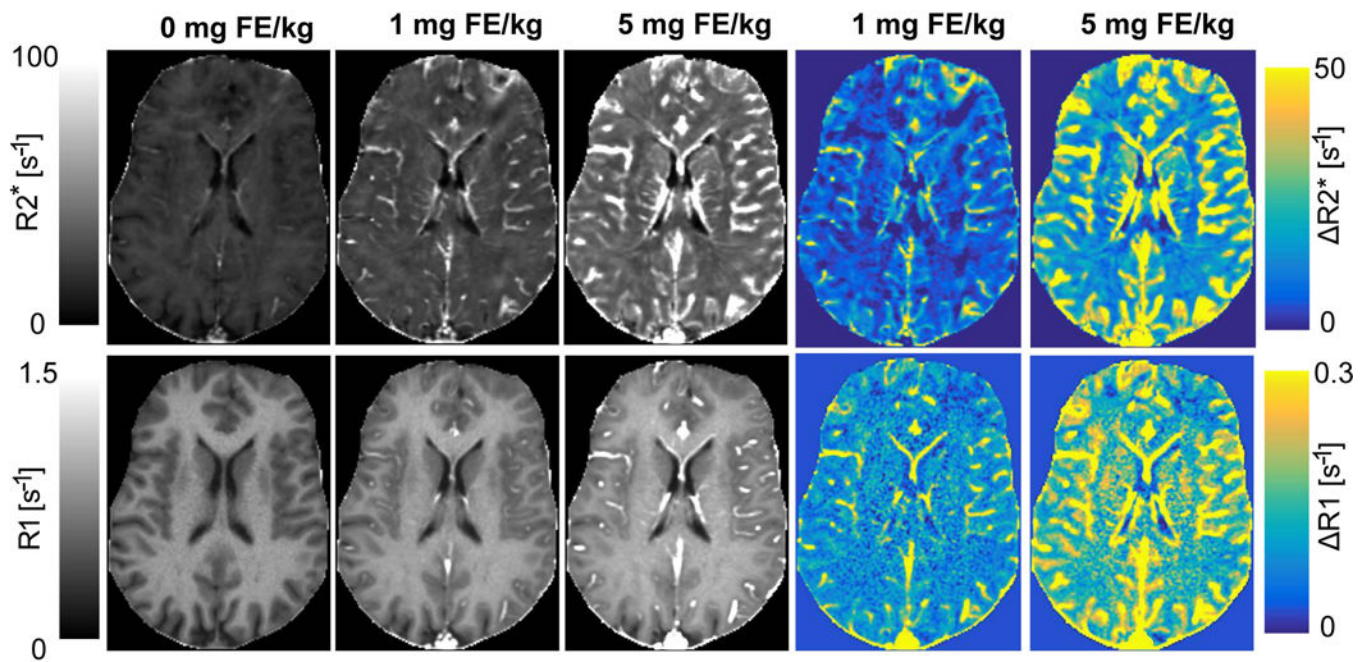
Figure 1.
Representative R2*, R1, ΔR2*, and ΔR1 maps from a single slice of the volume from one subject acquired with the UTE-VFA T1 and multi-echo T2* imaging techniques at different doses of ferumoxytol (0 mg FE/kg, 1 mg FE/kg, 5 mg FE/kg). R2* based imaging provides more sensitivity to signal; however, vessels are better depicted in R1 maps. R1 maps also demonstrate lower spatial distortions compared to R2* images. Some regional differences in ΔR1 and ΔR2* are observed, in this case in the frontal lobe gray and white matter, likely arising due to through plane blooming in R2* from vessels in adjacent slices.
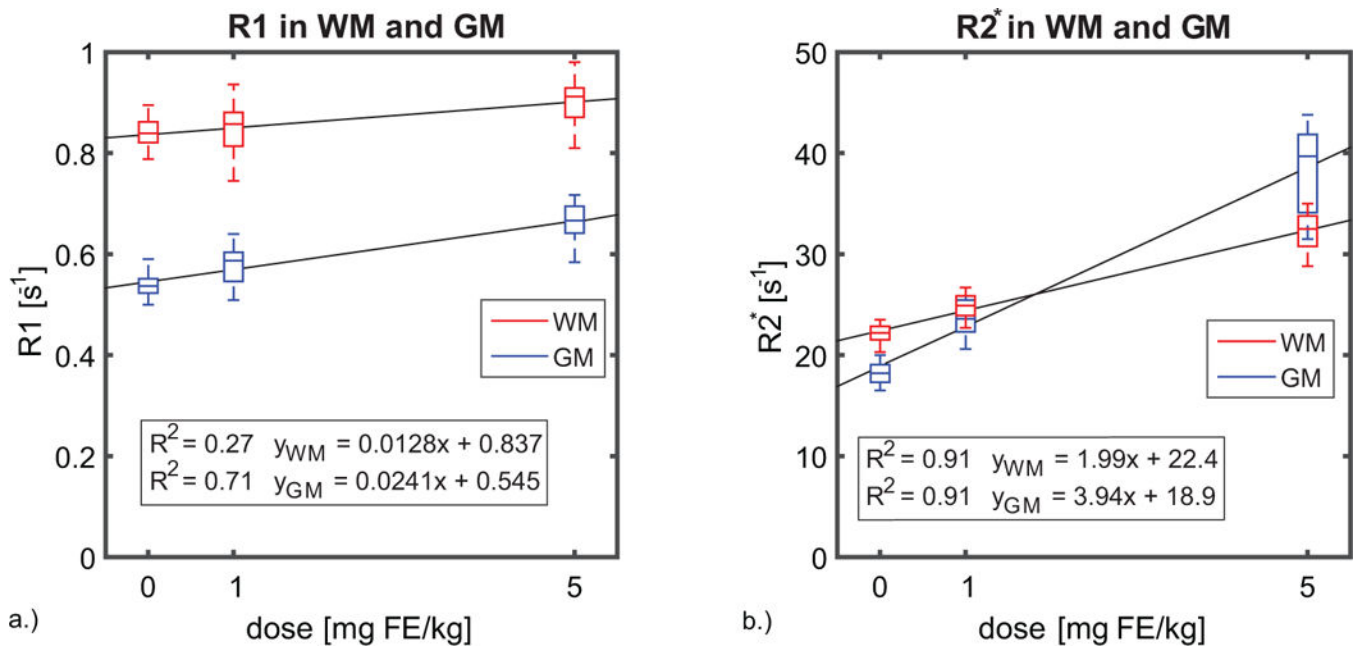
Figure 2.
Box plots displaying a.) the R1 and b.) R2* changes observed in all subjects (n=20) in gray matter and white matter. The R1 estimates show a weaker correlation with dose-response at high concentrations of ferumoxytol, with a coefficient of determination $R^2 = 0.27$ in WM and 0.71 in GM. While the R2* exhibits a stronger dose response in tissue having a coefficient of determination $R^2 = 0.91$ for both GM and WM.
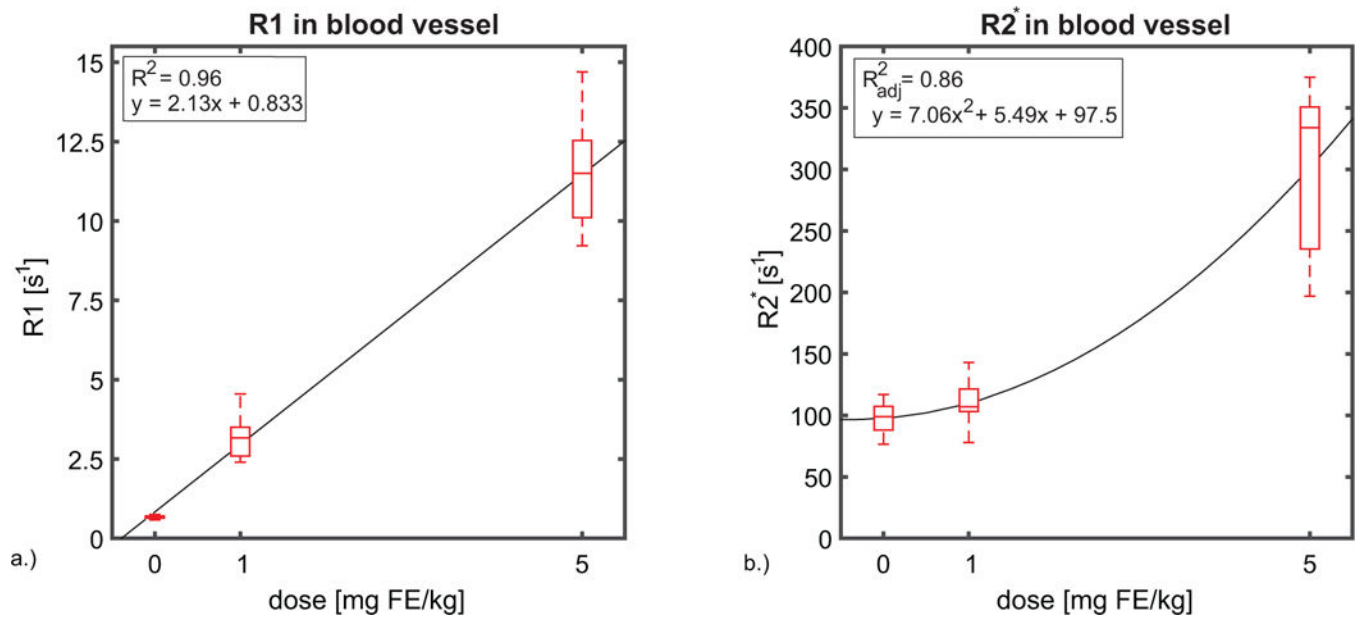
Figure 3.
Box plots showing the a.) R1 and b.) R2* changes observed in ROI's in a blood vessel (superior sagittal sinus) across all subjects (n=20). In large vessels, R1 in blood exhibits a linear response to dose of ferumoxytol with $R^2 = 0.96$ for the linear fit. While, R2* exhibits a non-linear response to dose, in contrast with a linear relationship between dose and R2* found in tissue. A quadratic model fit the data best with an adjusted coefficient of determination $R^2_{adj} = 0.86$. The superior sagittal sinus was selected to perform blood measurements in order to decrease the variance and possible sources of error. These sources of error include flow induced errors, B1 differences, B0 inhomogeneities and partial volume effects.
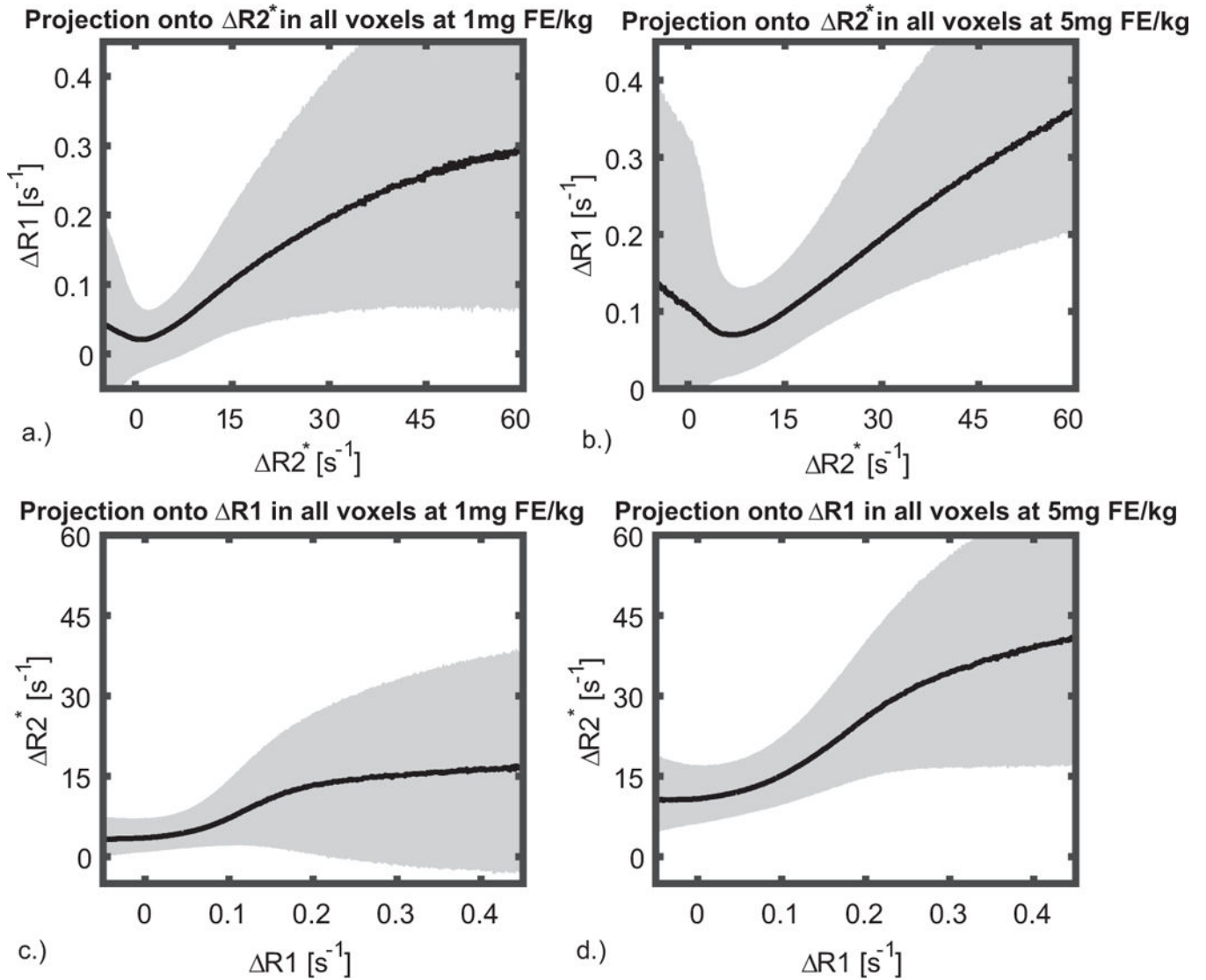
Figure 4.
Pixel wise relationship between ΔR2* and ΔR1 shown (a, d) for 1mgFE/kg and (b, d) 5mgFE/kg dose of ferumoxytol. The median is shown overlaid on 25–75% quartiles. The pixel wise correlation (a, b) shows a wide range of variation in ΔR1 where ΔR2* does not change. It should be noted that there are fewer voxels with these values, as partially indicated by the wider quartile range. When plotting ΔR2* vs ΔR1, ΔR2* (c, d) tends to exhibit changes where the ΔR1 does not change, suggesting the vessel size is overestimated in R2* images. Similarly, at high ΔR1, ΔR2* is weakly dependent on ΔR1. Many of these voxels are those containing small and medium sized vessels, where the dose response is non-linear and less sensitive to those in the capillary bed. These effects obfuscate the correlation of R2* and R1 outside of the homogenous tissues such as gray and white matter.
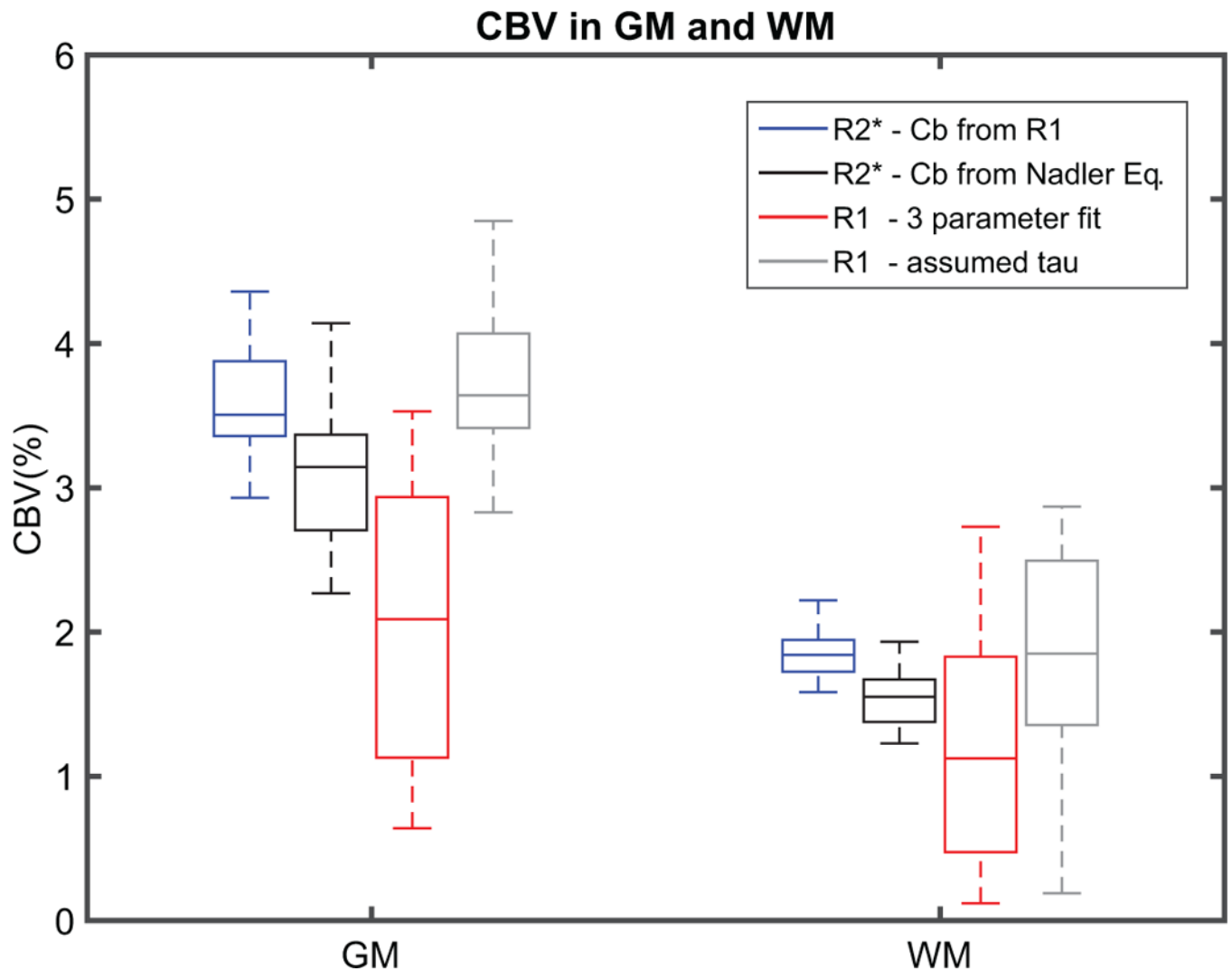
Figure 5.

Box plots showing different methods for CBV estimates in GM and WM across all subjects (n = 20). The CBV values were higher in both GM and WM when exploiting both: R2* linearity of ferumoxtyol in tissue using a steady state approach and blood R1 to estimate ferumoxytol concentration in blood (from left to right 1st box-blue). Similar but lower CBV estimates were found in GM and WM when using Nadler's equations to estimate ferumoxytol concentration in blood (2nd box-black). The CBV estimation from fitting 3 parameters into a two-compartment water exchange limited relaxation model were lowest in magnitude and higher in data spread for both GM and WM (3rd box-red). To investigate the spread of the data CBV was estimated from a 2 parameters fit assuming a value of $\tau_b = 0.233 \pm 0.012$ s (4th box-gray). Although the CBV estimates from the 2 parameter fit are forced by the R2* CBV estimates, the reduction in the spread of the data is real, revealing the PS product uncertainties will increase the spread of the CBV estimates.